



Photodegradation kinetics of organophosphorous with hydroxyl radicals: Experimental and theoretical study

SEYDA AYDOGDU¹, ARZU HATIPOGLU^{1*}, BAHAR EREN²
and YELDA YALCIN GURKAN²

¹*Yildiz Technical University, Department of Chemistry, 34220 Istanbul, Turkey*

²*Tekirdag Namik Kemal University, Department of Chemistry, 59030 Tekirdag, Turkey*

(Received 9 April, revised 28 June, accepted 29 June 2021)

Abstract: The presence of organophosphorus compounds (OPs) in the environmental counterparts has become an important problem because of their toxicity. In this study, the photocatalytic degradation reactions of the three OPs with hydroxyl radical were investigated by both experimental and quantum chemical methods. Photocatalytic degradation kinetics of the examined organophosphorus compounds were investigated under UV-A irradiation using TiO₂ as the photocatalyst. The effects of the initial concentrations on the degradation rate have been examined. There was an observable loss of OPs in the presence of TiO₂ photocatalyst under UV-A at 0.2 g TiO₂ per 100 mL. The quantum chemical calculations have been carried out by the density functional theory (DFT) at B3LYP/6-31g(d) level. The reaction pathways were modelled to find the most probable mechanism for OPs with the OH radical and to determine the primary intermediates. The rate constants of the eight reaction paths were calculated by the transition state theory. Conductor-like polarizable continuum model (CPCM) was used as the solvation model with the intention of understanding the water effect. The theoretical results were in agreement with experimental ones.

Keywords: UV-light; TiO₂; heterogenous catalysis; DFT; CPCM.

INTRODUCTION

Organophosphorous (OP) compounds are structurally characterized as esters or thiols derived from phosphoric, phosphonic, phosphinic or phosphoramidic acid.¹ They are mainly used as pesticides, lubricating agent, fuel additives and as warfare agents.² They are also used to synthesize the plasticizers.³ The OP's mechanism of action depend on their binding properties to the enzyme acetylcholinesterase at the nerve synapse in order to inhibite the hydrolysis of the neurotransmitter acetylcholine.⁴ Because of the effective properties of them as

*Corresponding author. E-mail: hatiparzu@yahoo.com
<https://doi.org/10.2298/JSC210409056A>

the pesticides, OPs are used in the worldwide extensively.⁵ the recent studies have demonstrated that only the 1 % of utilized OP compounds from the 4 million tones of used pesticides had reached the targed pest, and the rest of them distributed in the different environmental parts.⁶ Unfortunately, due to the widespread use, OP compunds have been detected in water, soil, even in the fruits and vegetables.⁷ It has been determined that the amount of OP in water is up to 506.6 $\mu\text{g L}^{-1}$.⁸ OPs pose serious threats to human health with harmful effects such as cytotoxicity, immunotoxicity, genotoxicity, and the joint effect of different OPs may become seriously toxic to health.⁹ In order to protect the public health, it is important to find effective methods of removing them from the environment.

In recent years, there are many methods used to eliminate organic contaminants in water.⁹ The advanced oxidation process (AOP) is the most important one of these methods. The main mechanism of this method is generating highly reactive radicals such as hydroxyl ($\cdot\text{OH}$) or sulfate radicals. The most reactive one is $\cdot\text{OH}$, which reacts with contaminants unselectively and fast. Their reaction is the dominant removal process of the contaminants in aquatic environment.⁴ Several researchers have studied the OP degradation with using AOPs. In some works, different parameters and newly prepared photocatalyst materials effect on the degradation reactions of OP compounds have been invesitigated. These studies have demonstrated the pozitive effects of increasing temperature and TiO_2 efficiency under UV irradiation light as a photocatalysis on the degradation of OP compounds.^{9–11} In the literature, there are also some studies that related the understanding of reaction mechanism and the detections of the intermediates of these reactions. With these studies, reserchers have tried to determine the toxicity of intermediates of OP compounds degradation reactions during the different AOP process. In these studies it has been found that the toxicities of transformation intermediates can be even more dangerous than the parent compounds.^{3,4,8,12,13} Though there are lots of studies about the degradation of OP compounds, it is still very limited to fully understand their reaction mechanism.

One alternative to experimental methods are the quantum chemical calculations. It is important to know the position of a radical attack on an organic molecule and how it will react.¹⁴ However, it is difficult to find out which atom in the molecule the radical will attack by only experimental methods.¹⁵ The quantum chemical calculations are suitable for deciding a reaction path and determining the transition states and products of the reaction by providing the correct potential energy surface.^{16,17} In literature, there are some theoretical research studies on the degradation reaction of the OP with the $\cdot\text{OH}$. In these studies, it has been showed that the hydrogen atom abstraction from the α carbon atom is a feasible reaction pathway.^{5,16–18} To the best of our knowledge, there are no studies performed on the photo-oxidative degradation reactions of dimethyl dimethyl phosphoramide (DDMP), diethyl phosphoramide (DEP) and isopro-

phyl phosphorous (ISPC). The molecular structure of DDMP, DEP and ISPC are shown in the Fig. 1.

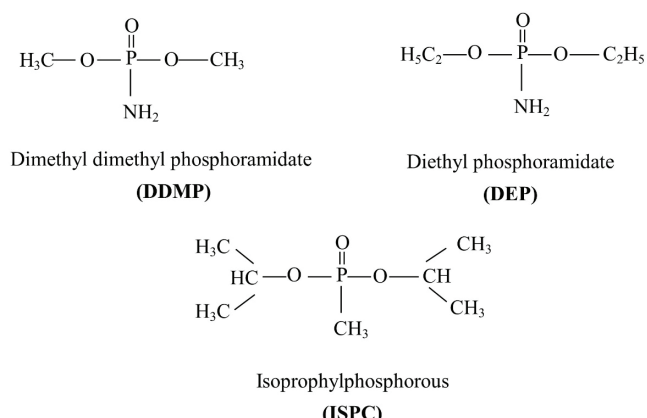


Fig. 1. Molecular structures of studied OPs.

In the experimental part of this study, the photodegradation kinetics of three OPs namely dimethyl dimethyl phosphoramide (DDMP), diethyl phosphoramide (DEP) and isopropylphosphorous (ISPC) have investigated in aqueous TiO₂ suspensions under UV irradiation. In the theoretical part, the calculations for all possible reaction paths have been performed by the quantum chemical density functional theory (DFT). Based on the results, the rate constants of the reactions were estimated by the transition state theory.

EXPERIMENTAL

Experimental methods

Materials. TiO₂ Degussa P25 grade with a particle size of about 21 nm and a surface area of 50 m² g⁻¹ was used as the photocatalyst without further treatment. Degussa P25 powder, which is a mixture of anatase and rutile phases (79 % anatase, 21 % rutile) is one of the photocatalysts with high activity and has been used as a standard TiO₂ reference material. The high activity is due to a synergistic effect between the two nanocrystalline phases.¹⁹ The OP molecules was purchased from Merck. All the chemicals that were used in the experiments were of laboratory reagent grade and used as received without further purification. The solutions were prepared with doubly distilled water.

Photocatalytic activity experiments. The performance of the OP molecules were assessed on TiO₂ by carrying out the photocatalytic degradation reactions. The photocatalytic activity experiments were carried out in a constant temperature batch-type photoreactor. 16×8 W blacklight fluorescent lamps were used as the light source. In the experiments, a stock solution of OP molecules, at a concentration of 10⁻² mol L⁻¹, was used. The suspension was prepared by mixing definite volumes of this solution containing the desired amount of OP molecules with TiO₂ Degussa P25. The suspension was agitated in an ultrasonic bath for 15 min in the dark before introducing it into the photoreactor. The volume of the suspension was 600 mL. The amount of the photocatalyst used was 0.2 g/100 mL, which was determined as the corres-

ponding optimum photocatalyst concentration. The suspension was stirred mechanically throughout the reaction period in order to prevent TiO₂ particles from settling. Owing to continuous cooling, the temperature of the reaction solution was 22±3 °C. All the samples, each 10 mL in volume were taken intermittently for analysis. The samples were then filtered through 0.45 µm cellulose acetate filters (Millipore HA WG04751). Before analyzing, all the solutions were wrapped by aluminum foil and kept in the dark. The concentration of OP molecules were measured by a UV–Visible spectrophotometer (Perkin Elmer Lambda 25) at 318 nm which was the wavelength of maximum absorption of OP molecules. The calibration curves were prepared for a concentration range (1.0–10.0)×10⁻⁵ mol L⁻¹. In the experiments, the pH of the reaction solution decreased slightly. For 100 min of degradation the change in the pH was ±0.3, which did not affect the wavelength of maximum absorption in the UV spectrum of OP molecules.

Computational methodology

The geometry optimizations of the reactants, the product radicals, the pre-reactives and the transition state complexes were determined with the density functional theory (DFT) within the Gaussian 09 package.²⁰ The DFT calculations were performed by B3LYP method which combines HF and Becke exchange term with Lee–Yang–Parr correlation functional with 6-31G(d) level.^{21,22} All the reactants, pre-reactive complexes and products confirmed as the stationary point with zero imaginary frequency. Whereas the transition states complexes were analyzed to be first order saddle points with the one negative eigenvalue that belong to the reaction coordinate by the frequency calculations. The forming O–H bond was chosen as the reaction coordinate for the determination of the transition states complexes for the OP + OH reactions. Intrinsic reaction coordinate (IRC) analysis were also carried out to prove the transition states really connected to expected reactants and the products.²³ In order to investigate the water effect the conductor-like polarizable continuum model (CPCM) was used. In this method, solute is placed in a cavity that surrounded by a polarizable continuum of solvent.²⁴

Rate constants of the reactions were calculated by using transition state theory (TST) for 273.15 K:

$$k = \frac{k_B T}{h} \frac{q_{TS}}{q_{OH} q_{OP}} e^{-E_a/RT} \quad (1)$$

In this equation, k_B is Boltzman constant, h is Plank constant, E_a is the activation energy and q 's are the molecular partition functions of reactants and transition states.²⁵ Each of the molecular partition functions are the products of translational, rotational, vibrational and electronic partition functions of all species. The overall rate constant of all investigated molecules reactions were obtained by the sum of all reaction path's rate constant.

RESULTS AND DISCUSSION

Experimental results

In this study, photocatalytic degradation reactions of OP molecules in aqueous TiO₂ suspensions were examined. When TiO₂, an n-type semiconductor, is irradiated with UV radiation, an electron from valence band (VB) jumps to the conduction band (CB), creating an electron–hole pair. Electron–hole pairs which formed in this way, can initiate oxidation and reduction reactions on the surface

of TiO_2 . In aqueous suspension systems, holes react with surface $-\text{OH}$ groups and generate $\cdot\text{OH}$. $\cdot\text{OH}$ is very reactive to OPs and degrades them.²⁶

Kinetics of DDMP, DEP and ISPC

Fig. 2 shows the disappearance kinetics of DDMP, DEP and ISPC from an initial concentration of $10^{-4} \text{ mol L}^{-1}$ under three conditions. In non-irradiated suspensions, there was a slight loss of three OPs, ~1.0 %, due to the adsorption onto TiO_2 particles. However, in the presence of TiO_2 , a rapid degradation of all of the studied OPs occurred by irradiation. The concentration change amounts to 83 and 90 % after irradiating for 90 min for DDMP and ISPC, respectively. For the DEP molecule the concentration change amounts to 87 % after irradiating for 100 min.

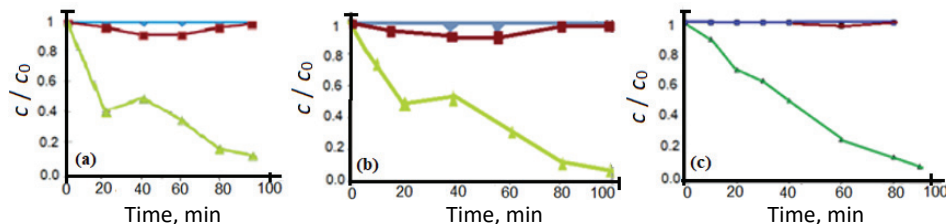


Fig. 2. Kinetics of the photocatalytic degradation of: a) DDMP, b) DEP and c) ISPC; (♦) photolysis, (■) adsorption in the dark, (►) photocatalysis.

The semilogarithmic plots of concentration data gave a straight line. The correlation constant for the fitted line for DDMP, DEP and ISPC were, $r = 0.9963$, 0.9788 and 0.9821 , respectively. This finding indicates that the photocatalytic degradation of OPs in aqueous TiO_2 suspensions can be described by the first-order kinetic model, $\ln c = -kt + \ln c_0$, where c_0 is the initial concentration and c is the concentration of the DDMP, DEP and ISPC at time t , respectively. Under the experimental conditions used, as explained above, the rate constant k for the degradation of DDMP, DEP and ISPC was calculated to be $(2.89 \pm 0.006) \times 10^{-8}$, $(1.78 \pm 0.008) \times 10^{-7}$, $(1.56 \pm 0.003) \times 10^{-10} \text{ min}^{-1}$, respectively.

Catalyst and initial concentration effect

The effect of the catalyst on the degradation rate is shown in Fig. 3. As the concentration of TiO_2 increased, the rate of degradation also increased up to a certain value of catalyst, then began to decrease slowly. The maximum degradation was obtained at $0.2 \text{ g (100 mL)}^{-1}$ TiO_2 concentration.

The initial concentration has a significant effect on the photocatalytic degradation rate, so the concentrations of OPs have been studied in the range $6\text{--}14 \text{ } 10^{-5} \text{ mol L}^{-1}$. The experimental results are presented in Fig. 4 and Table I, together with the correlation coefficients for each of the fitted lines. The results show that the degradation rate depends on the initial OPs concentrations. The rate

constant k increases with increase in the initial concentration of DDMP, DEP and ISPC. This finding indicates that the degradation kinetics of OPs is not of simple first order but pseudo-first order.

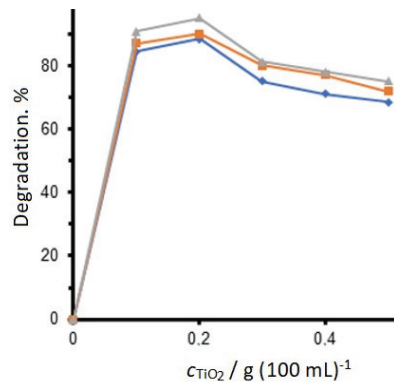


Fig. 3. The effect of TiO_2 concentration on the degradation rate, (◆) DDMP, (■) DEP, (▲) ISPC.

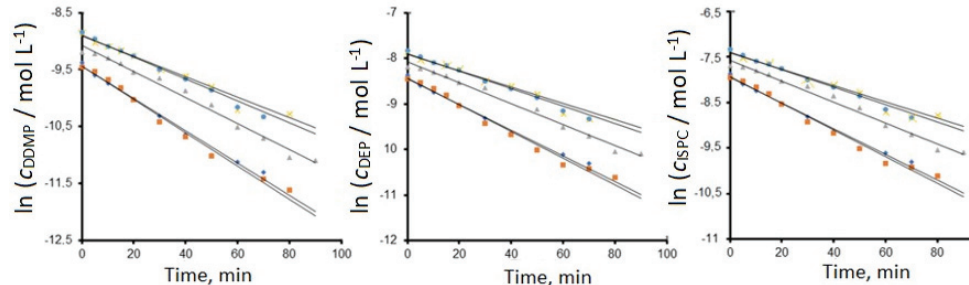


Fig. 4. Effect of the initial concentration on the degradation rate of DDMP, DEP and ISPC; (◆) 6×10^{-5} , (■) 8×10^{-5} , (▲) 10×10^{-5} , (×) 12×10^{-5} , (●) $14 \times 10^{-5} \text{ mol L}^{-1}$.

TABLE I. Apparent first-order rate constants k and correlation constant r for the photocatalytic degradation of OPs

Parameter	Initial concentration, $10^{-5} \text{ mol L}^{-1}$				
	6.0	8.0	10.0	12.0	14.0
DDMP					
$k / 10^{-8} \text{ min}^{-1}$	2.152±0.001	2.274±0.005	2.893±0.006	2.650±0.002	2.493±0.003
r	0.9914	0.9865	0.9963	0.9813	0.9943
DEP					
$k / 10^{-7} \text{ min}^{-1}$	1.353±0.004	1.462±0.006	1.784±0.008	1.672±0.005	1.550±0.001
r	0.9763	0.9811	0.9788	0.9877	0.9987
ISPC					
$k / 10^{-10} \text{ min}^{-1}$	1.390±0.009	1.431±0.008	1.561±0.003	1.514±0.001	1.481±0.006
r	0.9836	0.9916	0.9821	0.9614	0.9878

As can be seen from Table I, there was a slight increase in the reaction rate as the initial concentration increased from 6×10^{-5} to $8 \times 10^{-5} \text{ mol L}^{-1}$. However,

there was an observable increase in the reaction rate as the concentration increased from 8×10^{-5} to 1×10^{-4} mol L⁻¹. This indicated that the photodegradation degradation reaction occurs in solution as well as on the surface of TiO₂ particles. So, the initial concentration of OPs increases, the number of active sites on the TiO₂ surface decreases and the reaction rate changes accordingly.

Computational results

•OH is a strong electrophilic radical and it reacts with organic molecules directly.²⁷ It has a strong oxidizing potential with the value of $E(\text{OH}/\text{H}_2\text{O}) = 2.8$ V. •OH and OPs reactions occur mainly in two ways. The first one, the radical is able to abstract hydrogen from C–H and N–H bonds to form the water molecule. The second one, radical can make an addition to P=O bond.²⁸ In a previous study, it was found that the radical addition of organophosphorus to the P=O bond was not favourable because of the high activation energy.^{29,30} Thus, in this study only hydrogen abstraction reactions of •OH were taken into consideration.

DDMP+•OH reaction

DDMP+•OH degradation reaction pathways can take place with hydrogen abstraction from methyl groups, as shown in Fig. 5, where all the hydrogen atoms of the methyl group bonded to the same C atom are equivalent.

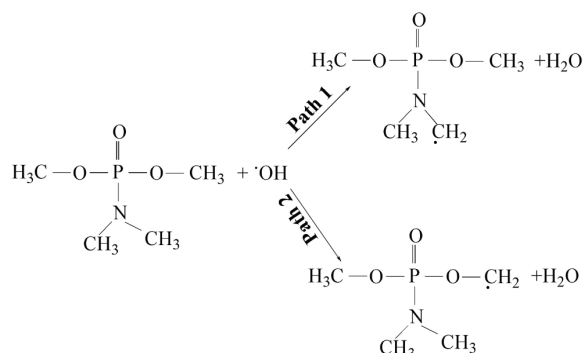


Fig. 5. Possible reaction pathways of the DDMP with •OH.

Pre-reactive complexes have important for the reaction mechanism due to the energies of the reactants. These complexes have weak van der Waals bonds. Such pre-reactive complexes affect the energy barrier of the reaction and the cleavage energies of its products as well as the kinetics.^{27,31}

The structural geometries all of the pre-reactive complexes are given in Fig. 6. In DDMP+•OH reaction two different pre-reactive complexes could occur. As it can be seen in the Fig. 6 for the PR1-DDMP structure, the oxygen atom of the hydroxyl radical approached the one of the hydrogen atom of the methyl group of DDMP molecule with the distance of 2.755 Å and the hydrogen atom of the

hydroxyl radical pointed toward the oxygen of DDMP molecule with the distance of 1.895 Å. These distances for PR2-DDMP were 2.398 and 1.806 Å, respectively. The angle of hydroxyl radical approaching to the DDMP molecule was almost 80.20° in both PR1-DDMP and PR2-DDMP.

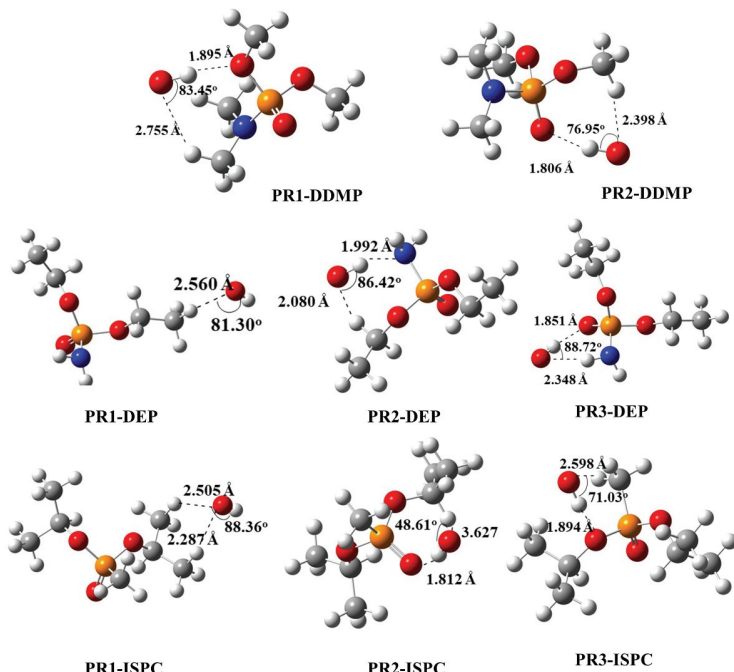


Fig. 6. The optimized structures of pre-reactive complexes at the B3LYP/6-31g(d) level.

There are two transition states for this reaction, TS1-DDMP and TS2-DDMP. The optimized geometries and the main geometrical parametres of transition states are given in the Fig. 7. As it can be seen in the Fig. 7, the major structural changes in the transition states of DMMP geometry for the breaking of the C–H bond was elongated, whereas the others stayed same. The elongation of breaking bond length of TS1-DDMP and TS2-DDMP were 0.143 and 0.106 Å, respectively. So TS1-DDMP is the early transition state. The C–O bond is of a critical length for the formation of the TS complex along the reaction coordinate. The C–O bond lengths of TS1 DDMP and TS2-DDMP were 1.44 and 1.40 Å, respectively. The shortening of C–N and C–O bond lengths of TS1 and TS2 were 0.028 and 0.006 Å, respectively.

The relative energies of the DDMP and reaction are given with Fig. 8. The energies of the TS complexes were 4.39 and 3.06 kcal* mol⁻¹ for gas and aqueous phase, respectively, as it can be seen in Fig. 8.

* 1 kcal = 4184 J

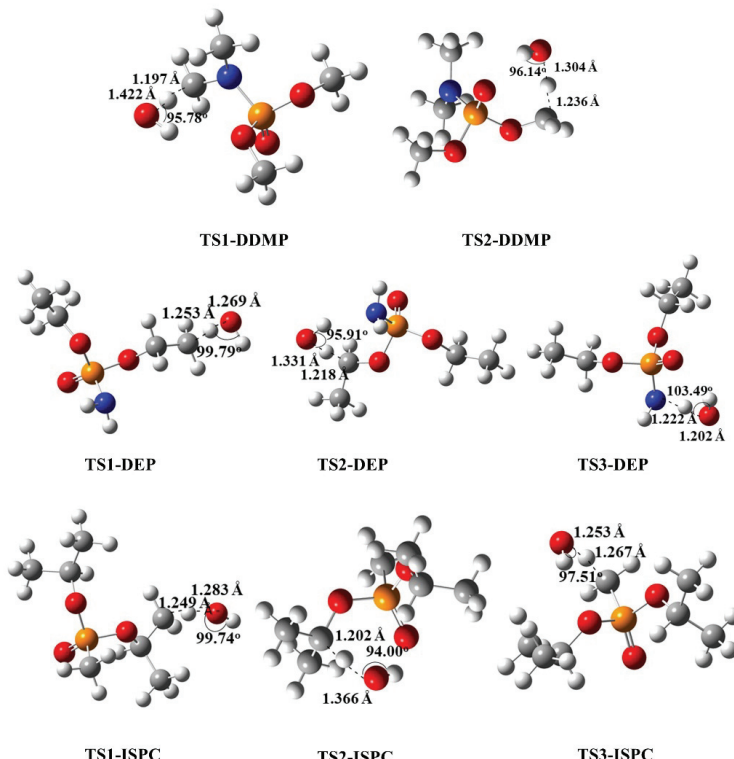


Fig. 7. The optimized structures of transition states complexes at the B3LYP/6-31g(d) level.

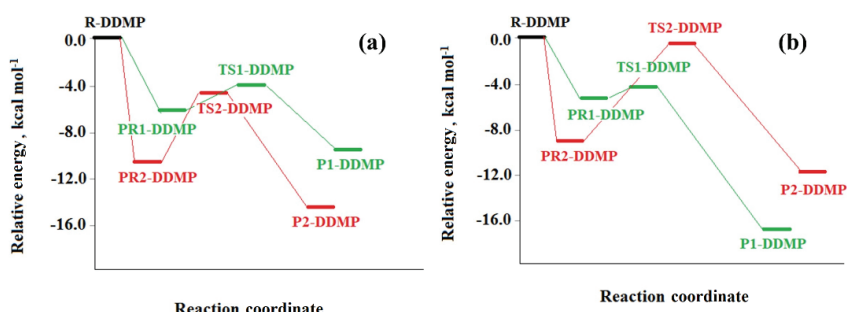


Fig. 8. Relative energies calculated at the B3LYP/6-31g(d) level of the reaction for DDMP+•OH: a) gas phase; b) aqueous medium.

In the aqueous phase the energies of TSs were decreased by around 7.98 kcal mol⁻¹ for TS1-DDMP and 6.47 kcal mol⁻¹ for TS2-DDMP in the gas phase. Thus, TS1 was the thermodynamically more stable complex (see Fig. 8). The energies of reactants, pre-reactive complexes, transition states and products for the all of the degradation reactions are given in the Supplementary material to this paper, as Tables S-I–S-III for both gas and aqueous phases.

The reaction heats of all the reactions are given in the Table II for both gas and aqueous phases, and both of reaction paths are exothermic. It may be concluded that Path 1 was the more probable reaction path, with the higher exothermicity for both phases. The values in Table II showed that the activation energy of Path 1 was 6.91 and 6.38 kcal mol⁻¹ lower than the Path 2, for the gas and aqueous phase, respectively. However, water has a stabilizing effect in terms of the energy barriers in aqueous solution. Energy barrier decreased 0.78 kcal mol⁻¹ in aqueous solution.

TABLE II. Calculated activation energies, reaction heats and rate constants of the reactions at the B3LYP/6-31g(d) level

Path	Gas			Aqueous		
	E_a kcal mol ⁻¹	ΔH kcal mol ⁻¹	k $\text{cm}^3 \text{molecule}^{-1} \text{s}^{-1}$	E_a 1	ΔH kcal mol ⁻¹	k $\text{cm}^3 \text{molecule}^{-1} \text{s}^{-1}$
DDMP						
Path 1	1.32	-18.34	1.73×10^{-8}	0.81	-17.00	1.43×10^{-7}
Path 2	8.23	-14.34	2.32×10^{-14}	7.19	-12.59	3.02×10^{-12}
Overall			1.73×10^{-8}			1.43×10^{-7}
DEP						
Path 1	3.01	-10.91	3.15×10^{-7}	4.70	-9.39	1.43×10^{-10}
Path 2	2.67	-17.62	2.53×10^{-10}	2.01	-16.20	2.49×10^{-10}
Path 3	9.78	-8.37	2.54×10^{-14}	9.39	-5.76	5.92×10^{-14}
Overall			3.15×10^{-7}			3.92×10^{-10}
ISPC						
Path 1	3.86	-10.80	1.26×10^{-8}	3.36	-9.32	2.86×10^{-10}
Path 2	2.60	-18.45	1.12×10^{-10}	1.77	-17.30	4.19×10^{-10}
Path 3	9.33	-11.01	1.88×10^{-14}	8.91	-9.56	2.96×10^{-14}
Overall			1.27×10^{-8}			7.05×10^{-10}

DEP+•OH reaction

There are three different abstractable hydrogen atoms for the DEP molecule, two from ethoxy groups and one from amino group. The reaction paths of DEP with •OH can be seen in Supplementary Fig. S-1.

There are three different pre-reactive complexes in these reaction, PR1-DEP, PR2-DEP and PR3-DEP. The optimized structures of pre-reactive complexes can be seen in the Fig. 6. •OH approached to the DEP molecule with the an angle 85.48°, which was almost the same for all three pre-reactive structures. The distances of oxygen of hydroxyl radical and hydrogen atom that were abstracted were 2.560, 2.080 and 2.348 Å for PR1-DEP, PR2-DEP and PR3-DEP, respectively.

There are three transition states for the reaction of DEP with •OH. The optimized structures of transition states TS1-DEP, TS2-DEP, TS3-DEP can be seen in Fig. 7. The distances between the oxygen atom of •OH and hydrogen of DEP

molecule were 1.269, 1.331 and 1.222 Å for TS1-DEP, TS2-DEP, TS3-DEP, respectively. According to the Hammond's Postulate, TS2-DEP was an early transition state with 0.348 Å, which is a higher elongation of occurring bond value.³² The calculated reaction enthalpies are listed on Table II. As seen in Table II, second reaction path was the one that prevailed with the highest exothermicity. For this reaction, the potential energy diagrams are given in Supplementary Fig. S-2 for both phases. As seen in the diagrams that the energy values of transition state structures were lower than those for the reactants for both phases, excluding TS1-DEP. This transition state's energy was approximately 3 kcal mol⁻¹ higher than reactants because of steric effect. The energy decreased for TS2- DEP and TS3- DEP were 4.29 kcal mol⁻¹ for gas and 3.35 kcal mol⁻¹ for DEP+•OH reaction. Comparing these three paths, Path 2 had the lowest activation energy, which was compatible with the thermodynamic results of the three reaction paths.^{33–35}

ISPC+•OH reaction

The degradation reaction paths of ISPC with •OH are given in Supplementary Fig. S-3. In this reaction, by the nature of the ISPC structure, hydroxyl radical could abstract three different hydrogen atoms. Thus, this reaction has three different reaction paths.

The pre-reactive complexes PR1-ISPC, PR2-ISPC and PR3-ISPC structures are given in Fig. 6. Among the pre-reactive complexes PR1-ISPC and PR3-ISPC are capable of forming a six-membered ring, while PR2-ISPC has the ability to form a seven-membered ring. This is the reason for the relative stability of these pre-reactive complexes compared to the reactant complexes. The oxygen of •OH approached to one of the hydrogen atoms of ISPC with the distances of 2.505, 3.627 and 2.598 Å for PR1-ISPC, PR2-ISPC and PR3-ISPC, respectively.

Depending on the •OH approach to ISPC, three different chemically activated transition states TS1-ISPC, TS2- ISPC and TS3- ISPC were determined. As displaced in Fig. 7, for all the transition states, •OH approached to the hydrogen atom with the angle, 99.74, 94.00 and 97.51° TS1-ISPC, TS2-ISPC and TS3- ISPC, respectively. Shortening of C–O bond in TS2-ISPC structure was 0.012 Å. There were also slight elongations of breaking bond, by around 0.109–0.175 Å, for all the transition state complexes. As can be seen in Fig. 7, among the all transition states, the longest O–H occurring bond length belonged to TS2-ISPC, while TS1-ISPC and TS3-ISPC have much lower as bond length when compared to TS2-ISPC, so, TS2-ISPC was an early transition state. The relative potential energy *versus* reaction coordinate diagrams for gas and aqueous phases are given in Supplementary Fig S-4. As seen in the diagrams, the energy values of transition state structures were higher than reactants for both phases excluding TS2- ISPC. This may be due to the branched structure of the ISPC. This transition

state complex were 9.14 and 5.56 kcal mol⁻¹ lower than the reactants for gas and aqueous phases, respectively. The energies of the transition states were around 7.34 kcal mol⁻¹ lower in the aqueous phase than in the gas phase. This can be attributed to the hydrogen bonds between ISPC and water molecules. Thus, the hydrogen bonding effect reduces the energies of these species. As can be seen from the Table II, the reaction paths were all exothermic and Path2 was the most exothermic one. This indicated that Path2 was the most probable hydrogen abstraction reaction from the ISPC with the lowest activation energy. This result is consistent with Zhou *et al.* result.¹⁸

Rate constants

The rate constant of all the studied reactions were given in the Table II. The calculated rate constants in Table II show that the highest rate constant belongs to DEP + •OH reaction. The rate constants were in the order $k_{DEP} > k_{DDMP} > k_{ISPC}$ for gas phase while in the aqueous medium order is $k_{DDMP} > k_{ISPC} > k_{DEP}$. The calculated rate constants showed that DDMP + •OH reaction proceeded slightly faster in aqueous medium in comparison to the gas phase. However, DEP+•OH and ISPC+•OH reaction rates decreased in aqueous solution. The reason may be attributed to their branched structure and the steric effect caused by it. Due to these structures, water molecules can have a weakening effect and the attack of the •OH radical to DEP and ISPC molecules in the aqueous environment can be sterically prevented.

As it can be seen in Table II, the reaction enthalpy change values are in agreement with the activation energies. For the DDMP+•OH reaction, the enthalpy change value and the activation energy of path 1 is lower (more exothermic) and this reaction pathway is faster than Path 2. There are 3 reaction pathways in the DEP+•OH and ISPC+•OH reactions. Of these paths, the most exothermic one is path 2 for both reactions. These pathways have the lowest activation energy and are the fastest in the aqueous medium. Whereas, in the gas phase the sequence is different. Though the Path 2 has the smallest activation energy for DEP and ISPC molecules' degradation reactions, they are not the fast ones. This may be attributed to the structure of the molecules. As can be seen in Fig. 6, for Path 1, it is easier to abstract the hydrogen atom at the end of the molecule. In Path 2, it is more difficult to abstract the hydrogen atom due to the steric hindrance. However, due to the branched structure, the hydrogen which should be abstracted in Path 2 is forming hydrogen bonds with neighboring atoms so it is difficult to abstract it.

CONCLUSION

In this work, the degradation kinetics of DDMP, DEP and ISPC were investigated both experimentally and theoretically. The photocatalytic degradation of DEP, DDMP and ISPC was investigated in aqueous TiO₂ suspensions with UV

light. The best degradation rate was obtained at 10^{-4} mol L⁻¹ initial concentration with UV/TiO₂. The experimental results indicated that the maximum degradation of DDMP, DEP and ISPC is due to photocatalysis at 0.2 g/100 mL TiO₂ concentration. Based on the DFT calculations results, the weakly bonded pre-reactive complexes were important for the degradation reactions because they were reducing the energy barrier. It has been found that the presence of a dielectric medium such as water has a stabilizing effect that reduces the total energy for this reaction system. The calculated rate constants show that for all of the reactions the rate decreases with the effect of hydrogen bonds in aqueous medium.

SUPPLEMENTARY MATERIAL

Additional data and information are available electronically at the pages of journal website: <https://www.shd-pub.org.rs/index.php/JSCS/article/view/10637>, or from the corresponding author on request.

Acknowledgement. The authors of this research have greatly acknowledged to financial support of Tekirdag Namik Kemal University Research Project with the project number of NKUBAP.01.GA.18.164.

ИЗВОД

КИНЕТИКА ФОТОДЕГРАДАЦИЈЕ ОРГАНОФОСФОРНИХ ЈЕДИЊЕЊА СА ХИДРОКСИЛ РАДИКАЛИМА: ЕКСПЕРИМЕНТАЛНО И ТЕОРИЈСКО ИСПИТИВАЊЕ

SEYDA AYDOGDU¹, ARZU HATIPOGLU¹, BAHAR EREN² и YELDA YALCIN GURKAN²

¹*Yildiz Technical University, Department of Chemistry, 34220 Istanbul, Turkey* и ²*Tekirdag Namik Kemal University, Department of Chemistry, 59030 Tekirdag, Turkey*

Присуство органофосфорних једињења (OF) у природи је важан проблем због њихове токсичности. У овом раду испитиване су реакције фотокаталитичке разградње три OF са хидроксил-радикалима експерименталним и квантотехничким методама. Кинетика фотокаталитичке разградње OF је испитивана применом UV-A зрачења и TiO₂ фотокатализатора. Испитивани су ефекти почетних концентрација на брзину разградње. Детектовано је смањење концентрације OF у присуству TiO₂ фотокатализатора при осветљавању са UV-A зрачењем при 0,2 g TiO₂/100 mL. Квантотехнички прорачуни су извршени применом теорије функционала густине (DFT) на B3LYP/6-31g(d) нивоу. Реакције су моделоване да би се одредио највероватнији механизам деградације OF са •OH и примарни интермедијери. Константе брзина осам реакција су израчунате помоћу теорије прелазног стања. *Conductor-like polarizable continuum model* (CPCM) је коришћен као солватациони модел да би се објаснио ефекат воде. Резултати теоријских разматрања су у сагласности са резултатима добијеним експерименталним методама.

(Примљено 9. априла, ревидирано 28. јуна, прихваћено 29. јуна 2021)

REFERENCES

1. M. B. Clovic, D. Z. Krstic, T. D. Lazarevic-Pasti, A. M. Bondvic, V. M. Vasic, *Curr. Neuropharmacol.* **11**(3) (2013) 315 (<https://pubmed.ncbi.nlm.nih.gov/24179466/>)
2. M. Lily, A. K. Chandra, *J. Fluor. Chem.* **175** (2015) 185 (<https://doi.org/10.1016/j.jfluchem.2015.04.019>)

3. H. Laversin, A. El Masri, M. Al Rashidi, E. Roth, A. Chakir, *Atmos. Environ.* **126** (2016) 250 (<https://doi.org/10.1016/j.atmosenv.2015.11.057>)
4. A. M. Parker, Y. Lester, E. M. Spangler, U. Gunten, K. G. Linden, *Chemosphere* **182** (2017) 477 (<https://doi.org/10.1016/j.chemosphere.2017.04.150>)
5. Q. Zhang, X. Qu, W. Wang, *Environ. Sci. Technol.* **41** (2007) 6109 (<https://pubmed.ncbi.nlm.nih.gov/17937289>)
6. Y. Zhou, Z. Yang, H. Yang, C. Zhang, X. Liu, *J. Mol. Model.* **23** (2017) 139 (<https://doi.org/10.1007/s00894-017-3277-0>)
7. L. Zhang, B. Li, X. Meng, L. Huang, D. Wang, *Environ. Sci. Pollut. Res.* **22** (2015) 15104 (<https://doi.org/10.1007/s11356-015-4669-2>)
8. W. Li, Y. Zhao, X. Yan, J. Duan, C. P. Saint, S. Beecham, *Chemosphere* **234** (2019) 204 (<https://doi.org/10.1016/j.chemosphere.2019.06.058>)
9. S. Agarwal, I. Tyagi, V. Kumar Gupta, M. H. Dehghani, A. Bagheri, K. Yetilmezsoy, A. Amrane, B. Heibati, S. Rodriguez-Couto, *J. Mol. Liq.* **221** (2016) 1237 (<https://doi.org/10.1016/j.molliq.2016.04.076>)
10. A. Almalraj, A. Pius, *J. Water Process. Eng.* **7** (2015) 94 (<https://doi.org/10.1016/J.JWPE.2015.06.002>)
11. C. Wu, K. G. Linden, *Water Res.* **44** (2010) 3585 (<https://doi.org/10.1016/j.watres.2010.04.011>)
12. A. Ozcan, Y. Sahin, M. A. Oturan, *Water Res.* **47** (2013) 1470 (<https://doi.org/10.1016/j.watres.2012.12.016>)
13. E. Evgenidou, I. Konstantinou, K. Fytianos, T. Albanis, *J. Hazard. Mater.* **137** (2006) 1056 (<https://doi.org/10.1016/j.jhazmat.2006.03.042>)
14. Q. Mei, J. Sun, D. Han, B. Wei, Z. An, X. Wang, J. Xie, J. Zhan, M. He, *Chem. Eng. J.* **373** (2019) 668 (<https://doi.org/10.1016/j.cej.2019.05.095>)
15. M. B. Kralj, P. Trebse, M. Franko, *Trends Anal. Chem.* **26** (11) (2007) 1020 (<https://doi.org/10.1016/j.trac.2007.09.006>)
16. J. Dang, L. Ding, X. Sun, Q. Zhang, W. Wang, *Struct. Chem.* **25** (2014) 275 (<https://doi.org/10.1007/s11224-013-0287-0>)
17. Y. Bao, C. Zhang, W. Yang, J. Hu, X. Sun, *Sci. Total Environ.* **419** (2012) 144 (<https://doi.org/10.1016/j.scitotenv.2012.01.004>)
18. Q. Zhou, X. Sun, R. Gao, J. Hu, *Atmos. Environ.* **45** (2011) 3141 (<https://doi.org/10.1016/j.scitotenv.2014.10.081>)
19. P. Bouras, E. Stathatos, P. Lianos, *Appl. Catal., B* **73** (2007) 51 (<https://doi.org/10.1016/j.apcatb.2006.06.007>)
20. Gaussian 09, Revision A.02, Gaussian, Inc., Wallingford, CT, 2009
21. A. D. Becke, *J. Chem. Phys.* **98** (1993) 5648 (<https://doi.org/10.1063/1.464913>)
22. C. Lee, W. Yang, R. G. Parr, *Phys. Rev., B* **37** (1988) 785 (<https://doi.org/10.1103/physrevb.37.785>)
23. C. Gozalez, H. B. Schlegel, *J. Phys. Chem.* **94** (1990) 5523 (<https://doi.org/10.1021/j100377a021>)
24. D. C. Young, *Computational Chemistry*, 2nd ed., John Wiley & Sons, Inc., New York, 2001
25. I. N. Levine, *Physical Chemistry*, 6th ed., Mc Graw Hill Higher Education, New York, 2009
26. N. Sam, A. Hatipoğlu, G. Koçtürk, Z. Çınar, *J. Photochem. Photobiol., A* **146** (2002) 189 ([https://doi.org/10.1016/S1010-6030\(01\)00620-7](https://doi.org/10.1016/S1010-6030(01)00620-7))

27. A. Hatipoglu, D. Vione, Y. Yalçın, C. Minero, Z. Çınar, *J. Photochem. Photobiol., A* **215** (2010) 59 (<https://doi.org/10.1016/j.jphotochem.2010.07.021>)
28. Y. Zhou, X. Liu, W. Jiang, Y. Shu, *J. Mol. Model.* **24** (2018) 44 (<https://doi.org/10.1007/s00894-018-3580-4>)
29. C. Li, S. Zheng, J. Chen, H. Xie, Y. Zhang, Y. Zhao, Z. Du, *Chemosphere* **201** (2018) 557 (<https://doi.org/10.1016/j.chemosphere.2018.03.034>)
30. Ş. Aydoğdu, A. Hatipoğlu, *J. Indian Chem. Soc.* **96** (2019) 1117
31. N. Mora-Diez, R. J. Alvarez-Idaboy, R. J. Boyd, *J. Phys. Chem., A* **105** (2001) 9034 (<https://doi.org/10.1021/jp011472i>)
32. B. S. Hammond, *J. Am. Chem. Soc.* **77** (1955) 334 (<https://doi.org/10.1021/ja01607a027>)
33. E. A. Kozlova, P. G. Smirniotis, A. V. Vorontsov, *J. Photochem. Photobiol., A* **162** (2004) 503 ([https://doi.org/10.1016/S1010-6030\(03\)00392-7](https://doi.org/10.1016/S1010-6030(03)00392-7))
34. A. V. Vorontsov, D. V. Kozlov, P. G. Smirniotis, V. N. Parmon, *Kinet. Catal.* **46** (2005) 189 (<https://doi.org/10.1007/s10975-005-0067-y>)
35. B. Yang, Y. Wang, J. Shu, P. Zhang, W. Sun, N. Li, Y. Zhang, *Chemosphere* **138** (2015) 966 (<https://doi.org/10.1016/j.chemosphere.2014.12.039>).